Research Article | Vol. 25, No. 19 | 18 Sep 2017 | OPTICS EXPRESS 22947
Optics EXPRESS

Analysis of a lens-array modulated coaxial holographic data storage system with considering recording dynamics of material

YEH-WEI YU,[1] CHI-HSIANG YANG,[2] TSUNG-HSUN YANG,[1,2] SHIUAN-HUEI LIN,[3] AND CHING-CHERNG SUN[1,2,3,*]

[1]*Optical Sciences Center, National Central University, Chung-Li, 320 Taiwan*
[2]*Department of Optical and Photonics, National Central University, Chung-Li, 320 Taiwan*
[3]*Department of Electrophysics, National Chiao Tung University, Hsin-Chu, Taiwan*
[*]*ccsun@dop.ncu.edu.tw*

Abstract: In the first time, a simulation model with considering the recording dynamics of material is built and is used to simulate evolution of the grating strength of the recorded hologram in a coaxial volume holographic memory system. In addition, phase modulation by lens array in the reference is introduced and observed to perform better diffracted signal quality and higher shifting selectivity, in both simulation and experiment. The use of lens array is found to provide multiple advantages in volume holographic memory system. The new simulation model potentially can be used to precisely design the system to obtain higher diffracted signal quality, higher shifting selectivity, and reduction of M# consumption and increase of storage capacity.

OCIS codes: (210.0210) Optical data storage; (090.2900) Optical storage materials; (210.2860) Holographic and volume memories.

References and links

1. T. Hoshizawa, K. Shimada, K. Fujita, and Y. Tada, "Practical angular-multiplexing holographic data storage system with 2 terabyte capacity and 1 gigabit transfer rate," Jpn. J. Appl. Phys. **55**(9S), 09SA06 (2016).
2. L. Dhar, K. Curtis, and T. Fäcke, "Holographic data storage: Coming of age," Nat. Photonics **2**(7), 403–405 (2008).
3. M. Gu, X. Li, and Y. Cao, "Optical storage arrays: a perspective for future big data storage," Light Sci. Appl. **3**(5), e177 (2014).
4. E. N. Leith, A. Kozma, J. Upatnieks, J. Marks, and N. Massey, "Holographic data storage in three-dimensional media," Appl. Opt. **5**(8), 1303–1311 (1966).
5. L. Hesselink, S. S. Orlov, and M. C. Bashaw, "Holographic data storage systems," IEEE **92**(8), 1231–1280 (2004).
6. H. Horimai, X. Tan, and J. Li, "Collinear holography," Appl. Opt. **44**(13), 2575–2579 (2005).
7. K. Tanaka, H. Mori, M. Hara, K. Hirooka, A. Fukumoto, and K. Watanabe, "High density recording of 270 Gbits/inch^2 in a coaxial holographic storage system," Tech. Digest of ISOM 2007, MO–D–03.
8. K. Curtis, L. Dhar, A. Hill, W. Wilson, and M. Ayres, *Holographic Data Storage: From Theory to Practical Systems* (Wiley, 2010).
9. K. Anderson and K. Curtis, "Polytopic multiplexing," Opt. Lett. **29**(12), 1402–1404 (2004).
10. R. Fujimura, T. Shimura, and K. Kuroda, "Multiplexing capability in polychromatic reconstruction with selective detection method," Opt. Express **18**(2), 1091–1098 (2010).
11. T. Ochiai, D. Barada, T. Fukuda, Y. Hayasaki, K. Kuroda, and T. Yatagai, "Angular multiplex recording of data pages by dual-channel polarization holography," Opt. Lett. **38**(5), 748–750 (2013).
12. J. Zang, G. Kang, P. Li, Y. Liu, F. Fan, Y. Hong, Y. Huang, X. Tan, A. Wu, T. Shimura, and K. Kuroda, "Dual-channel recording based on the null reconstruction effect of orthogonal linear polarization holography," Opt. Lett. **42**(7), 1377–1380 (2017).
13. G. Barbastathis, M. Levene, and D. Psaltis, "Shift multiplexing with spherical reference waves," Appl. Opt. **35**(14), 2403–2417 (1996).
14. H. Y. S. Li and D. Psaltis, "Three-dimensional holographic disks," Appl. Opt. **33**(17), 3764–3774 (1994).
15. T. C. Teng, Y. W. Yu, and C. C. Sun, "Enlarging multiplexing capacity with reduced radial cross talk in volume holographic discs," Opt. Express **14**(8), 3187–3192 (2006).
16. T. Nobukawa, Y. Wani, and T. Nomura, "Multiplexed recording with uncorrelated computer-generated reference patterns in coaxial holographic data storage," Opt. Lett. **40**(10), 2161–2164 (2015).

#298010 https://doi.org/10.1364/OE.25.022947
Journal © 2017 Received 14 Jun 2017; revised 7 Sep 2017; accepted 8 Sep 2017; published 12 Sep 2017

Optics EXPRESS

17. C. Li, L. Cao, Z. Wang, and G. Jin, "Hybrid polarization-angle multiplexing for volume holography in gold nanoparticle-doped photopolymer," Opt. Lett. **39**(24), 6891–6894 (2014).
18. J. Li, L. Cao, H. Gu, X. Tan, Q. He, and G. Jin, "Orthogonal-reference-pattern-modulated shift multiplexing for collinear holographic data storage," Opt. Lett. **37**(5), 936–938 (2012).
19. L. Cao, J. Liu, J. Li, Q. He, and G. Jin, "Orthogonal reference pattern multiplexing for collinear holographic data storage," Appl. Opt. **53**(1), 1–8 (2014).
20. C. C. Sun and W. C. Su, "Three-dimensional shifting selectivity of random phase encoding in volume holograms," Appl. Opt. **40**(8), 1253–1260 (2001).
21. F. H. Mok, G. W. Burr, and D. Psaltis, "System metric for holographic memory systems," Opt. Lett. **21**(12), 896–898 (1996).
22. L. P. Yu, W. Chan, Z. Bao, and S. X. F. Cao, "Synthesis and physical measurements of a photorefractive polymer," J. Chem. Soc.-Chem. Comm. **7**(23), 1735–1737 (1992).
23. M. R. Ayres and R. R. McLeod, "Medium consumption in holographic memories," Appl. Opt. **48**(19), 3626–3637 (2009).
24. S. S. Orlov, W. Phillips, E. Bjornson, Y. Takashima, P. Sundaram, L. Hesselink, R. Okas, D. Kwan, and R. Snyder, "High-transfer-rate high-capacity holographic disk data-storage system," Appl. Opt. **43**(25), 4902–4914 (2004).
25. T. Nobukawa and T. Nomura, "Multilevel recording of complex amplitude data pages in a holographic data storage system using digital holography," Opt. Express **24**(18), 21001–21011 (2016).
26. J. Joseph and D. A. Waldman, "Homogenized Fourier transform holographic data storage using phase spatial light modulators and methods for recovery of data from the phase image," Appl. Opt. **45**(25), 6374–6380 (2006).
27. Y. W. Yu, C. Y. Chen, and C. C. Sun, "Increase of signal-to-noise ratio of a collinear holographic storage system with reference modulated by a ring lens array," Opt. Lett. **35**(8), 1130–1132 (2010).
28. S. Yasuda, Y. Ogasawara, J. Minabe, K. Kawano, M. Furuki, K. Hayashi, K. Haga, and H. Yoshizawa, "Optical noise reduction by reconstructing positive and negative images from Fourier holograms in coaxial holographic storage systems," Opt. Lett. **31**(11), 1639–1641 (2006).
29. K. Tanaka, M. Hara, K. Tokuyama, K. Hirooka, K. Ishioka, A. Fukumoto, and K. Watanabe, "Improved performance in coaxial holographic data recording," Opt. Express **15**(24), 16196–16209 (2007).
30. Y. W. Yu, S. Xiao, C. Y. Cheng, and C. C. Sun, "One-shot and aberration-tolerable homodyne detection for holographic storage readout through double-frequency grating-based lateral shearing interferometry," Opt. Express **24**(10), 10412–10423 (2016).
31. S. R. Lambourdiere, A. Fukumoto, K. Tanaka, and K. Watanabe, "Simulation of Holographic Data Storage for the Optical Collinear System," Jpn. J. Appl. Phys. **45**(2B), 1246–1252 (2006).
32. K. Kuroda, Y. Matsuhashi, R. Fujimura, and T. Shimura, "Theory of polarization holography," Opt. Rev. **18**(5), 374–382 (2011).
33. J. Wang, G. Kang, A. Wu, Y. Liu, J. Zang, P. Li, X. Tan, T. Shimura, and K. Kuroda, "Investigation of the extraordinary null reconstruction phenomenon in polarization volume hologram," Opt. Express **24**(2), 1641–1647 (2016).
34. C. Li, L. Cao, Q. He, and G. Jin, "Holographic kinetics for mixed volume gratings in gold nanoparticles doped photopolymer," Opt. Express **22**(5), 5017–5028 (2014).
35. B. A. Kowalski, A. C. Sullivan, M. D. Alim, and R. R. Mcleod, "Predictive modeling of two-component holographic photopolymers," Proc. SPIE **10233**, 10233N (2017).
36. T. Shimura, S. Ichimura, R. Fujimura, K. Kuroda, X. Tan, and H. Horimai, "Analysis of a collinear holographic storage system: introduction of pixel spread function," Opt. Lett. **31**(9), 1208–1210 (2006).
37. T. Shimura, Y. Ashizuka, M. Terada, R. Fujimura, K. Kuroda, "What Limits the Storage Density of the Collinear Holographic Memory." Tech. Digest of ODS2007,TuD1.
38. C. C. Sun, Y. W. Yu, S. C. Hsieh, T. C. Teng, and M. F. Tsai, "Point spread function of a collinear holographic storage system," Opt. Express **15**(26), 18111–18118 (2007).
39. Y. W. Yu, T. C. Teng, S. C. Hsieh, C. Y. Cheng, and C. C. Sun, "Shifting selectivity of collinear volume Holographic storage," Opt. Commun. **283**(20), 3895–3900 (2010).
40. C. C. Sun, "A simplified model for diffraction analysis of volume holograms," Opt. Eng. **42**(5), 1184–1185 (2003).
41. S. H. Lin, Y. N. Hsiao, and K. Y. Hsu, "Preparation and Characterization of Irgacure 784 Doped Photopolymers for Holographic Data Storage at 532 nm," J. Opt. A, Pure Appl. Opt. **11**(2), 024012 (2009).
42. K. Y. Hsu, S. H. Lin, Y. N. Hsiao, and W. T. Whang, "Experimental Characterization of Phenanthrenequinone-Doped Poly(methyl methacrylate) Photopolymer for Volume Holographic Storage," Opt. Eng. **42**(5), 1390–1396 (2003).
43. J. Mumbru, I. Solomatine, D. Psaltis, S. H. Lin, K. Y. Hsu, W. Z. Chen, and W. T. Whang, "Comparison of the recording dynamics of phenanthrenequinone-doped poly (methyl methacrplate) materials," Opt. Commun. **194**(1-3), 103–108 (2001).

1. Introduction

Volume holographic memory (VHM) has been extensively studied for its potential in data storage for the advantages including high storage density, high access rate, multiple

Optics EXPRESS

multiplexing schemes, long life and energy saving [1–8]. The advantage of multiplexing scheme allows multiple storage pages recorded at the same location of the holographic medium [9–20]. The intrinsic characteristic of the recording medium in holographic data storage is that the refractive index change corresponding to holographic exposure fringe is large enough to offer the diffracted signal i *test* n acceptable signal-to-noise ratio (SNR). Accordingly, a so-called M-number (M#) is useful to indicate the storage capacity, which depends on refractive index change and the thickness of the recording medium. M# is related to the diffraction efficiency (η) of each stored hologram when N holograms are multiplexed in the same volume [21,22],

$$\eta = \frac{M\#^2}{N^2}. \tag{1}$$

Because the final diffraction efficiency of each elementary hologram is as small as possible, Eq. (1) can be further written

$$M\# = N\Delta n_e L, \tag{2}$$

where Δn_e is the corresponding refractive index change for each elementary hologram, and L is the effective length of the hologram. From Eq. (2), M# is proportional to the product of number of hologram stored in the medium with the minimum refractive index change in each elementary hologram, and it is equivalent the potentially largest refractive index change of the recording medium. When the recording medium performs larger refractive index change and larger thickness, the M# is larger. It means that more holograms with sufficient diffraction efficiency can be stored in the medium. Once the geometry and medium of holographic disc is determined, the M# is determined. Then a very important issue is how to reduce consumption of M# in designing a VHM system [23–25]. Although there are studies discussing proper ways to utilize the given M# and enlarge the number of the stored hologram, the optimized condition depends on the detailed design of the VHM system. One of general approaches is to improve the mixing uniformity of the signal and the reference inside the recording material. For example, Polytopic architecture is proposed to eliminate the inter-page cross-talk and block the signal noise [9]. For this architecture, phase spatial light modulator is used to remove the strong peak at the focus [26]. However, the reference beam exposures some regions without signal beam and causes extra M# consumption [23]. Coaxial VHM system uses high-spatial-frequency phase modulation or phase encoded methods to remove the strong peak at the focus [27–30]. However, the reference beam and the signal beam is separated before they reach the focal plane of the objective lens [31]. Since the mixing ratio gets worse with shorter objective focal-length or with thicker recording material, the system storage capacity is limited. Even saving M# is an important issue; however, there is lack of an efficient study in analyzing the diffracted signal with considering the material reaction. Since the mathematical model of both recording material and optical system have been reported in many literatures, the mathematical link between recording material and the optical system is highly demanded [32–40]. In this paper, we first build up a precise calculation model incorporating the material function to predict diffracted image and also to check M# consumption. Then a new encoded way for the coaxial VHM system is proposed and analyzed for its diffracted image quality with respect to the material function.

2. Theoretical model

The holographic recording disc in a coaxial VHM system is located at the back focal plane of the first objective lens (Obj_1). The signal (S) and the reference (R) are both encoded at the same spatial light modulator (SLM), but the reference is a ring structure surrounding the signal. The signal and the reference interferes at the focal plane of the objective lens, and the interference pattern is recorded by the holographic medium with refractive index change in

Optics EXPRESS

correspondence. The reading (probing) beam is encoded with the same pattern as the reference while there is no signal in the readout process.

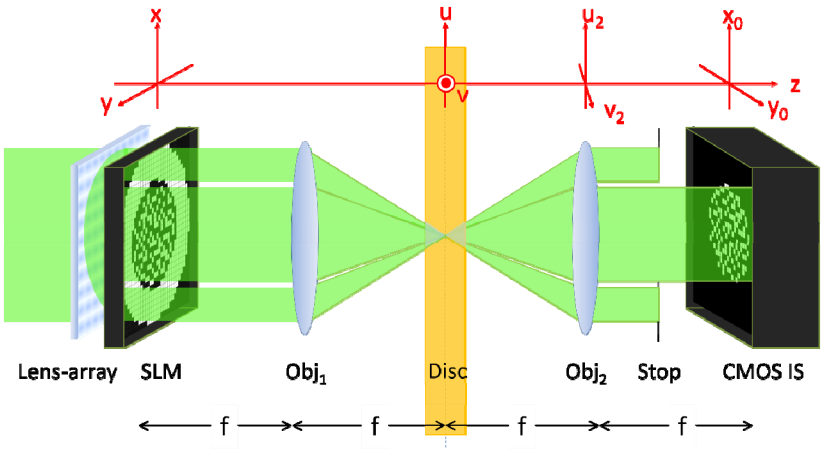

Fig. 1. The simplified optical model of the coaxial VHM system.

Figure 1 shows the typical simplified optical model of a coaxial VHM system [36, 38]. The optical fields of the signal, reference and the reading beam in the disc can be written respectively

$$R(\mathrm{u},\mathrm{v},\Delta z)=\frac{e^{jk\left(2f+\Delta z\right)}}{j\lambda f}\Im\left\{U_R(x,y)\mathrm{e}^{-j\frac{\pi\Delta z}{\lambda f^2}\left(x^2+y^2\right)}\right\}\Bigg|_{\substack{\frac{u}{\lambda f}\\ \frac{v}{\lambda f}}}, \tag{3}$$

$$S(\mathrm{u},\mathrm{v},\Delta z)=\frac{e^{jk\left(2f+\Delta z\right)}}{j\lambda f}\Im\left\{U_S(x,y)\mathrm{e}^{-j\frac{\pi\Delta z}{\lambda f^2}\left(x^2+y^2\right)}\right\}\Bigg|_{\substack{\frac{u}{\lambda f}\\ \frac{v}{\lambda f}}}, \tag{4}$$

$$P(\mathrm{u},\mathrm{v},\Delta z)=\frac{e^{jk\left(2f+\Delta z\right)}}{j\lambda f}\Im\left\{U_P(x,y)\mathrm{e}^{-j\frac{\pi\Delta z}{\lambda f^2}\left(x^2+y^2\right)}\right\}\Bigg|_{\substack{\frac{u}{\lambda f}\\ \frac{v}{\lambda f}}}, \tag{5}$$

where $\Im$ is the Fourier transform operator; λ is the optical wavelength; f is the focal length of the objective lenses; k is the wave number; and Δz is the distance deviated from the focal plane of the objective lens along z axis. At the SLM plane, U_R, U_S and U_P are the electrical field of the reference, signal and reading beams, respectively. To simplify the calculation model, each

Optics EXPRESS

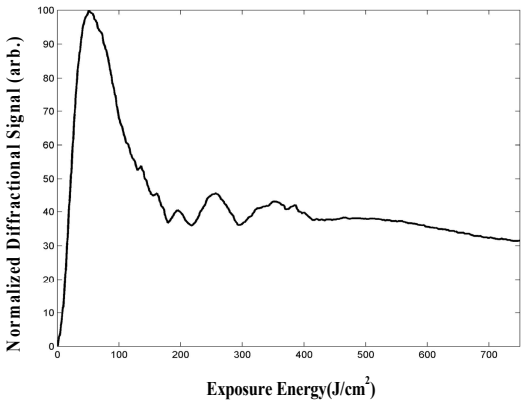

Fig. 2. The measured diffraction efficiency of PQ/PMMA as a function of exposure energy.

elementary hologram in the medium can be regarded as an elementary unit performing a complex amplitude transmittance

$$t_A \propto I = |R+S|^2 . \tag{6}$$

However, such an assumption does not take the material response of the recording medium in consideration, and the grating strength as well as M# consumption is not well monitored. An alternative equation with recording dynamics of material (RDM) is expressed

$$t_A \propto I = \mathrm{RDM}\left(|R+S|^2\right). \tag{7}$$

where RDM is the measured diffraction efficiency as a function of exposure energy of PQ/PMMA as shown in Fig. 2 [41–43]. Here, the hologram was recorded by using two plane waves with s-polarization from a solid state laser with wavelength of 532 nm. The angle between two plane waves is 30 degree. The intensity of each wave is 50 mW/cm^2. We monitored the diffraction efficiency of the hologram during recording by a weak 632-nm beam from a He-Ne laser. As mentioned in Ref [42], the PQ:PMMA materials have reasonably wide spatial-frequency response, the curve shown in Fig. 2 can also represent the material response for other recording angles from 10 to 50 degrees. In addition, with the physical mechanism of holographic recording in PQ/PMMA proposed in Ref [43], that the recording dynamics is mainly conducted by competition of two out of phase gratings, it is reasonable to model the experimental curve in Fig. 2 as the following formula,

$$\eta = \sin^2\left[\frac{2\pi T}{\lambda}\Delta n(E)\right], \tag{8}$$

and

$$\Delta n(E) = A_1 \times \left(1 - \mathrm{e}^{\frac{E}{E_{\tau 1}}}\right) - A_2 \times \left(1 - \mathrm{e}^{\frac{E}{E_{\tau 2}}}\right), \tag{9}$$

where η is diffraction efficiency of hologram, λ is wavelength, T is thickness of recording material, Δn is the refractive index change of the hologram, E is exposure energy density. The dynamics of Δn can be written as Eq. (9), in which A_1 and A_2 are saturated grating amplitude of two gratings, respectively. $E_{\tau 1}$ and $E_{\tau 2}$ are growth time constants of two gratings during recording. These four parameters can be extracted by curve fitting and the mathematical formula of Eq. (8) can be used in the simulation.

Optics EXPRESS

Equation (7) connects the diffraction efficiency and the exposure energy which is a consuming factor of M#. Then the strength of each grating can be monitored and the consumption of M# becomes clearer. Based on Eq. (7), the diffracted light can be expressed

$$U_d(u,v,\Delta z) = P(u,v,\Delta z)\cdot \mathrm{RDM}\left(\left|R(u,v,\Delta z)+S(u,v,\Delta z)\right|^2\right), \tag{10}$$

The diffracted light being propagated to the back plane of the second objective lens (Obj_2) is written

$$U''(u_2,v_2,\Delta z) = \frac{e^{jk(f-\Delta z)}}{j\lambda(f-\Delta z)}\int_{-\infty}^{\infty}\int_{-\infty}^{\infty} U_d(u,v,\Delta z). \cdot e^{j\frac{k}{2(f-\Delta z)}\left[(u_2-u)^2+(v_2-v)^2\right]}dudv \tag{11}$$

Passing through the second objective lens, the optical field of the diffracted light is written

$$U'(u_2,v_2,\Delta z) = U''(u_2,v_2,\Delta z)e^{-j\frac{k}{2f}\left(u_2^2+v_2^2\right)}. \tag{12}$$

The diffracted light by the elementary hologram on each single layer of the recording medium is expressed

$$U_l(\mathrm{x}_0,\mathrm{y}_0,\Delta z) = \frac{e^{jkf}}{j\lambda f}\int_{-\infty}^{\infty}\int_{-\infty}^{\infty} U'(u_2,v_2,\Delta z). \cdot e^{j\frac{k}{2f}\left[(x_0-u_2)^2+(y_0-v_2)^2\right]}du_2dv_2 \tag{13}$$

Equation (13) can be expanded as

$$U_l(\mathrm{x}_0,\mathrm{y}_0,\Delta z) = -(\lambda f)^2 e^{j\pi\frac{8f^3-\Delta z(\mathrm{x}_0^2+\mathrm{y}_0^2)}{\lambda f^2}}\cdot\left\{\left\{\mathrm{e}^{j\frac{\pi\Delta z}{\lambda f^2}(\mathrm{x}_0^2+\mathrm{y}_0^2)} \cdot U_p(-\mathrm{x}_0,-\mathrm{y}_0)\right\}\otimes\Im\left\{\mathrm{RDM}\left[\left|R(u,v,\Delta z),+S(u,v,\Delta z)\right|^2\right]\right\}\Big|_{\substack{\mathrm{x}_0\\ y_0}}\right\} \tag{14}$$

where ⊗ denotes convolution operation. Based on VOHIL model [20, 40], we sum up the diffracted lights from all the elementary holograms in every layer, and the complete diffracted light can be written

$$U_{\mathrm{det}}(\mathrm{x}_0,\mathrm{y}_0) = -(\lambda f)^2\int_{-T/2}^{T/2}\mathrm{e}^{j\frac{8\pi\mathrm{f}}{\lambda}-j\frac{\pi\Delta z}{\lambda f^2}(\mathrm{x}_0^2+\mathrm{y}_0^2)}\cdot\left\{\left\{U_p(-\mathrm{x}_0,-\mathrm{y}_0)\cdot\mathrm{e}^{j\frac{\pi\Delta z}{\lambda f^2}(\mathrm{x}_0^2+\mathrm{y}_0^2)}\right\}\otimes\Im\left\{\mathrm{RDM}\left[\left|R(u,v,\Delta z)+S(u,v,\Delta z)\right|^2\right]\right\}\Big|_{\substack{\mathrm{x}_0\\ y_0}}\right\}d\Delta z \tag{15}$$

Optics EXPRESS

Through the readout process, the holographic disc is rotated and then the diffracted light moves laterally, e.g., *a*, *b*, with respect to the CMOS image sensor (CMOS IS), and then the optical field is expressed

$$U_{\mathrm{det}}(\mathrm{x}_0,\mathrm{y}_0)=-(\lambda f)^2\int_{-T/2}^{T/2}\mathrm{e}^{j\frac{8\pi \mathrm{f}}{\lambda}-j\frac{\pi\Delta z}{\lambda f^2}(\mathrm{x}_0{}^2+\mathrm{y}_0{}^2)}\cdot\left\{\left\{U_p(-\mathrm{x}_0,-\mathrm{y}_0)\cdot\mathrm{e}^{j\frac{\pi\Delta z}{\lambda f^2}(\mathrm{x}_0{}^2+\mathrm{y}_0{}^2)}\right\}\otimes\left\{\mathrm{e}^{-j\frac{4\pi}{\lambda f}(a\,\mathrm{x}_0+b\,\mathrm{y}_0)}\cdot\Im\left\{\mathrm{RDM}\left[\left|R(u,v,\Delta z)+S(u,v,\Delta z)\right|^2\right]\right\}\Big|_{\substack{\mathrm{x}_0\\ y_0}}\right\}\right\}d\Delta z. \tag{16}$$

In comparison with previous calculation models, Eq. (16) provides a different insight in calculating diffraction efficiency with considering RDM of the exposure. Without the material function, we cannot monitor each grating strength and know the consumption of M#.

3. Simulation of coaxial VHM system improved by lens-array modulation

The experiment was designed with coaxial VHM system as shown in Fig. 3, where the reference and the signal are modulated by the SLM. The reflected light is relayed and focused at the back focal plane of the objective lens, which is at the reflecting plane of the recording medium. In a general approach, the reference is a ring structure. Then a strong focus spot can be found in the recording plane. The focus spot forms a sharp irradiance distribution across the recording medium, and the reference and the signal only mixes to each other near the reflecting plane. When the recording layer leaves from the reflecting plane, the reference and the signal separate dramatically. Therefore, the grating strength varies across the volume of the recording medium and only a few recording materials are utilized. To improve the mixing uniformity and mixing ratio, several approaches were proposed, including binary random phase encoding [29] and lens array modulation [27]. Both the approaches encode the reference with additional phase in high spatial frequency. The latter is reported to perform better image quality in the readout signal.

In this paper, the study will focus on the lens array phase modulation. A 532-nm continuous-wave laser (Verdi-V5, Coherent Inc.) is used as the light source. In contrast to the pervious design, the lens array plate (Edmund Optics, microlenses array; 10 × 10mm in size; 500μm in pitch) is imaged to the SLM (Jasper Display JD8554SDK; 1920 × 1080 pixels; 6.4-μm pixel size) plane, so that the phase modulated by the lens array covering the whole SLM. Each effective pixel of the input encoded signal uses 4 × 4 SLM pixels, and 3:16 sparse code is applied to the encoded image. The focal length of L1, L2, L3, L4, and L5 are 90mm, 105mm, 200mm, 180mm, and 200mm. The focal length and numerical aperture of the objective lens is 4mm and 0.75, respectively. The readout signal is detected by the CMOS image sensor (IDS UI306xCP-M; 1936 × 1216 pixels; 5.86-μm pixel size). The thickness of the disk is 0.5mm. In this paper, MATLAB is the software platform used for the simulations.

Optics EXPRESS

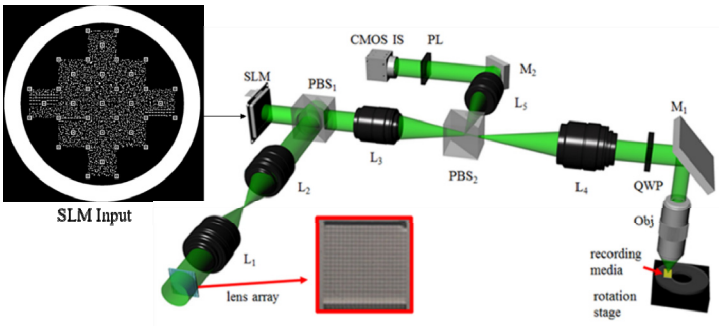

Fig. 3. The experiment setup, where the modulated phase of the lens array is imaged to the SLM. L: lens, PBS: polarized beam splitter, M: mirror, QWP: quarter wave plate, Obj: objective lens, PL: polarizer.

Figure 4 shows a simulation of the readout signal for the cases without and with lens array modulation when the material function is not considered. The case in lens array modulation is much better than that without phase modulation because the Bragg-degeneration from neighboring reference-pixels is suppressed. It leads to better point spread function, and thus contributes to better image quality [36, 38]. However, such a simulation does not reflect the fact that grating strength is a function of exposure energy. If the material repose function is considered, as in Eq. (16), we can simulate the diffracted signal for different exposure time, as shown in Fig. 5. We applied the RDM of the PQ/PMMA, as shown in Fig. 1. The recording power and the reading power is 1.81mW and 1.20mW, respectively. For the case without lens-array, there exists an optimized exposure time (1s in Fig. 5) to perform better signal quality. In that condition, some of the gratings are over exposure and the diffracted signal becomes weaker from the maximum, and some of them are in insufficient exposure energy, so that the overall image quality becomes fair. However, it is a waste of M# due to over exposure. In contrast, in the case of lens array modulation, the strength in all grating segments are similar. Then the required image quality can be obtained under minimum energy consumption. The control of exposure time balances the image quality and M# consumption. This is the important role of material function in the simulation model. Figure 5 shows the experiment results comparing with the simulation result. The parameters of the experiment and the simulation are exactly the same. It shows both the simulation can predict the experimental result well. When recording exposure-time is equal to 3 sec., both lens-arrays show the ability to smooth the over-exposure effect. When recording exposure-time is as large as 60 sec., even the lens array (focal-length = 46.7mm) is applied, the recording medium contributing to central part of diffracted signal is still saturate. Only the lens array (focal-length = 13.8mm) can suppress the over-exposure effect. However, the shorter focal length, the more critical to align the lens array. In this paper, we choose 13.8mm as the shortest focal length in this study.

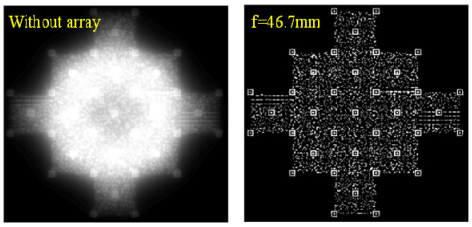

Fig. 4. Simulation of the readout signal for (a) without lens array, and (b) with the lens array with focal length of 46.7mm.

Optics EXPRESS

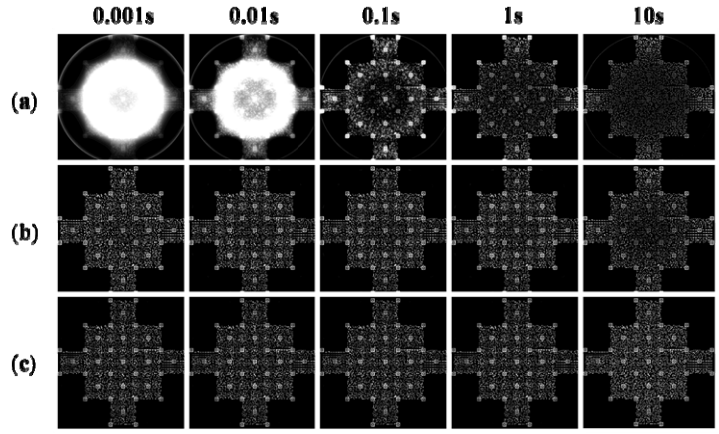

Fig. 5. Simulation of the diffracted signal based on Eq. (16) for different exposure time. (a) without lens array, (b) with the lens array with focal length of 46.7mm, and (c) with the lens array with focal length of 13.8mm.

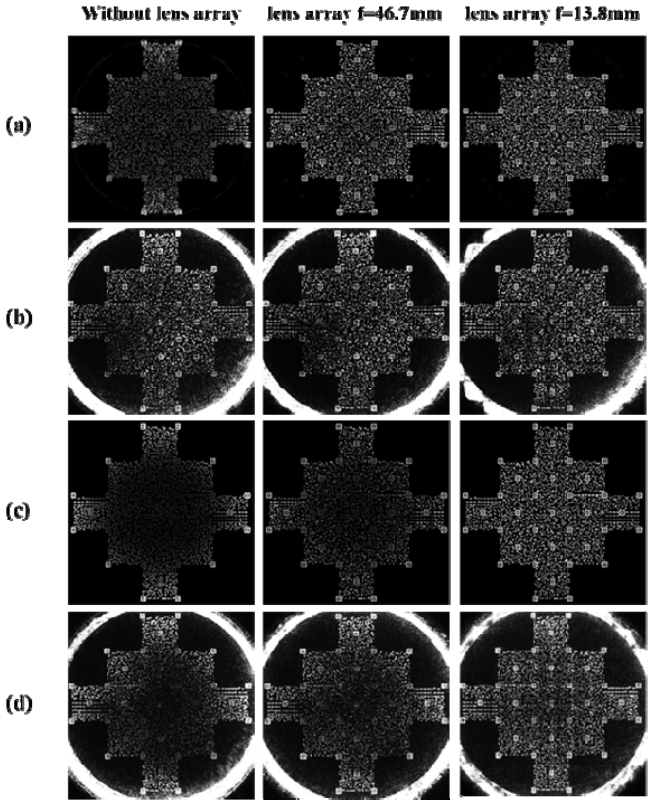

Fig. 6. The diffracted signals for different lens-arrays applied with the recording exposure time of (a) 3 sec. (simulation), (b) 3 sec. (experiment), (c) 60 sec. (simulation), and (d) 60 sec. (experiment).

4. Shifting selectivity

The use of lens array has multiple benefits in a coaxial VHM system. Figure 5&6 shows the benefit in uniform spread of grating strength to obtain better image quality of the readout signal and also minimum illumination energy can be made in considering M# consumption.

Optics EXPRESS

Another benefit is that uniform spread of the signal and reference beams across the volume of the recording medium leads to high mixing ratio and high mixing uniformity, and will make the geometry of each recorded elementary hologram thicker. Then the shifting selectivity becomes higher. In contrast, in the case without lens-array, the recorded hologram gets different strength at different location for different exposure time. The geometry of the elementary hologram is equivalently thinner, so that lower shifting selectivity is performed. The result decreases the recording capacity of the recording medium. Figures 7&8 show a comparison of the readout signals in two cases in simulation and experiment when the holographic disc is laterally shifted. Both of the simulation and experiment show that lens-array modulation performs higher selectivity than the general ring reference does.

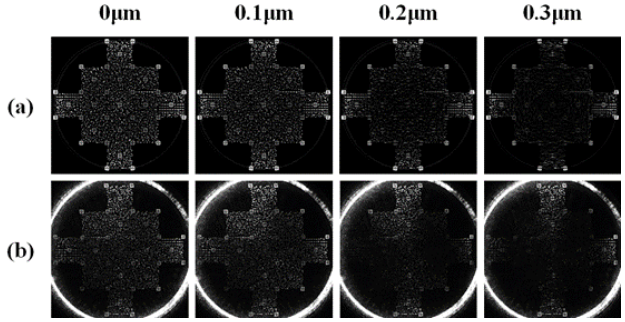

Fig. 7. In the case without lens array, the diffracted signals for different lateral displacement in (a) simulation, and (b) the corresponding experiment.

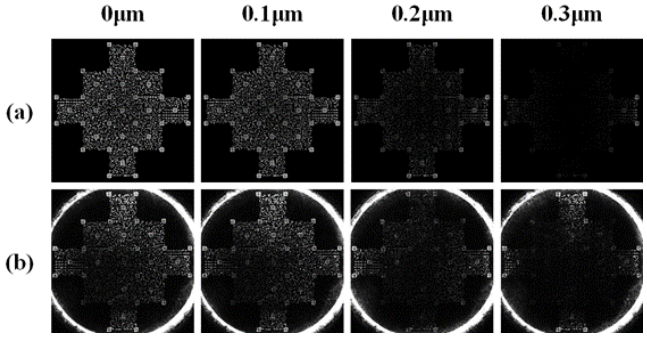

Fig. 8. In the case of lens array reference, the diffracted signals for different lateral displacement in (a) simulation, and (b) the corresponding experiment.

The simulation with Eq. (15) and the corresponding experiment show that the lens array modulation is an effective way to enhance grating uniformity, easy to obtain optimal exposure time, and to perform higher shifting selectivity. Then to know the effect of the lens parameter is important to optimize the performance of the lens array. The focal length of the lens array is the key parameter because it affects the uniformity of the grating strength in both the lateral and longitudinal directions. Figure 9 shows a comparison of the normalized diffraction signal intensity vs. lateral displacement in the readout process. The blue line indicates the simulation result, and the red and green lines indicate two times of measurement with the same experimental condition to ensure validity of the simulation. With no doubt, the case with lens array modulation is better than which without lens array modulation. We also can find that the focal length of the lens array is also important. The focal length of 13.8mm performs higher shifting selectivity than that of 46.7mm. The lens in higher NA effectively mixes the signal and reference across the recording volume of the medium. In contrast, without lens array, it cannot effectively mix the reference and signal laterally and longitudinally. Thus M# is greatly wasted. This phenomena is more obvious when the recording medium is thicker.

Optics EXPRESS

Figure 10 shows a comparison among the three VHM systems for different thickness (0.5mm and 1mm) of the holographic recording medium. In the general ring reference, the reference light always mixes the outer part of the signal. The condition becomes worse when the disc is thicker. The lens array modulation dramatically improves quality of the diffracted signal, and the lens with higher NA performs better diffracted signal.

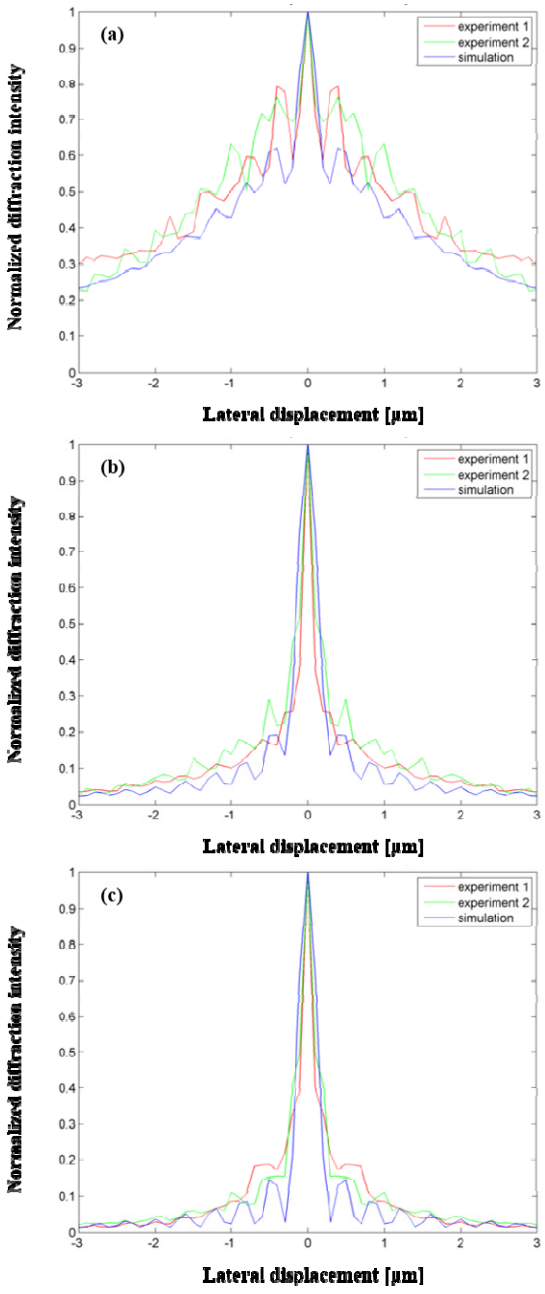

Fig. 9. The normalized selectivity in simulation (blue line) and the corresponding measurement (red &green lines) in the cases of (a) the general ring reference, (b) lens array reference with the focal length of 46.7mm, and (c) of 13.8mm.

Optics EXPRESS

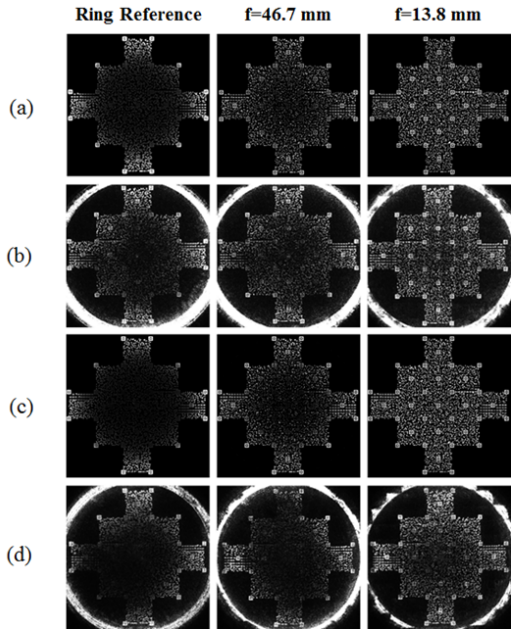

Fig. 10. The diffracted signals for different references with the medium thickness of (a) 0.5mm (simulation), (b) 0.5mm (experiment), (c) 1mm (simulation), and (d) 1mm (experiment).

5. Conclusion

The exposure response of a holographic recording medium is a key factor in designing a VHM system. Generally, M# is an indication of RDM and how to reduce waste of M# becomes important. In an un-optimized coaxial VHM system, worse mixing uniformity and mixing ratio cause waste of M#. This condition, however, cannot be simulated if RDM is not considered. In this paper, we first modify the previous model with the aid of RDM in the new simulation equation. Then we apply two kinds of lens array with different focal lengths to perform better diffracted signal, and also to save the M#. `

The simulation first shows the evolution of the grating strength by evaluating the cases without lens array and the case with lens array. The former performs large variation in the diffracted signal quality, and the latter performs high quality of the diffracted signal. Besides, the simulation is also applicable to select the proper exposure time and to save the M#. It ensures the required image quality can be obtained under minimum energy consumption.

Owing to improved mixing ratio and mixing uniformity across the recording medium, the effective record volume in which with lens array is larger than which without lens array. The result is that higher shifting selectivity is performed, as shown in simulation and the corresponding experimental result. When we enlarge the NA of the lens-array by shortening the focal length to 13.8mm, higher shifting selectivity and higher diffracted signal quality in a thicker recording medium can be observed. The use of lens array reference is shown to perform multiple advantages in the coaxial VHM system. The new simulation model effectively predicts the behaviors and can be used to optimize the design of the system by considering the diffracted signal quality and M# consumption.

Funding

Ministry of Education National Central University's Plan to Develop First-class Universities and Top-level Research Centers (103G-903-2); Grants from the Ministry of Science and Technology Taiwan (MOST 104-2221-E-008-073-MY3; MOST 105-2218-E-008 –013 -MY3).